



Article

# A Global Picture of Molecular Changes Associated to LPS Treatment in THP-1 Derived Human Macrophages by Fourier Transform Infrared Microspectroscopy

Diletta Ami <sup>1</sup>, Ana Rita Franco <sup>1</sup> , Valentina Artusa <sup>1</sup> , Paolo Mereghetti <sup>2</sup>, Francesco Peri <sup>1</sup> and Antonino Natalello <sup>1,\*</sup>

<sup>1</sup> Department of Biotechnology and Biosciences, University of Milano-Bicocca, Piazza della Scienza 2, 20126 Milan, Italy

<sup>2</sup> Independent Researcher, 15061 Arquata Scrivia, Italy

\* Correspondence: antonino.natalello@unimib.it

**Abstract:** Macrophages are among the first immune cells involved in the initiation of the inflammatory response to protect the host from pathogens. THP-1 derived macrophages (TDM) are used as a model to study the pro-inflammatory effects of lipopolysaccharide (LPS) exposure. Intact TDM cells were analysed by Fourier transform infrared (FTIR) microspectroscopy, supported by multivariate analysis, to obtain a snapshot of the molecular events sparked by LPS stimulation in macrophage-like cells. This spectroscopic analysis enabled the untargeted identification of the most significant spectral components affected by the treatment, ascribable mainly to lipid, protein, and sulfated sugar bands, thus stressing the fundamental role of these classes of molecules in inflammation and in immune response. Our study, therefore, shows that FTIR microspectroscopy enabled the identification of spectroscopic markers of LPS stimulation and has the potential to become a tool to assess those global biochemical changes related to inflammatory and anti-inflammatory stimuli of synthetic and natural immunomodulators different from LPS.

**Keywords:** biomarkers; inflammation; infrared microspectroscopy; lipopolysaccharide; multivariate analysis; THP-1 derived macrophages



**Citation:** Ami, D.; Franco, A.R.; Artusa, V.; Mereghetti, P.; Peri, F.; Natalello, A. A Global Picture of Molecular Changes Associated to LPS Treatment in THP-1 Derived Human Macrophages by Fourier Transform Infrared Microspectroscopy. *Int. J. Mol. Sci.* **2022**, *23*, 13447. <https://doi.org/10.3390/ijms232113447>

Academic Editor: Antonio Palumbo Piccionello

Received: 6 October 2022

Accepted: 30 October 2022

Published: 3 November 2022

**Publisher's Note:** MDPI stays neutral with regard to jurisdictional claims in published maps and institutional affiliations.



**Copyright:** © 2022 by the authors. Licensee MDPI, Basel, Switzerland. This article is an open access article distributed under the terms and conditions of the Creative Commons Attribution (CC BY) license (<https://creativecommons.org/licenses/by/4.0/>).

## 1. Introduction

Inflammation is a key host response that ensures protection against injury or infection. In the case of microbial infection, the innate immune system plays a very important role in the initiation of the inflammatory response. It can recognize highly conserved pathogen-associated molecular patterns (PAMPs) through different specialised receptors, thus starting a cascade of pro-inflammatory events in order to protect the host from the pathogen [1]. Among the first lines of cellular defence against infection, macrophages are extremely plastic cells able to rapidly change their functional profile through a process defined as polarisation. Polarisation is the process by which macrophages respond to stimuli coming from the local microenvironment and acquire a specific functional phenotype [2].

Classical activated macrophages, described as the M1 phenotype, are part of this local non-specific response to PAMPs as they are able to produce pro-inflammatory cytokines such as TNF- $\alpha$ , IL-6 and IL-1 $\beta$ , and also have microbicidal activity. Alternatively activated macrophages, M2 phenotype, are characterised by an anti-inflammatory profile which permits resolution of inflammation and tissue repair [3]. One of the PAMPs responsible for M1 activation is lipopolysaccharide (LPS), the major component of the outer leaflet of the gram-negative bacteria outer membrane, which strongly activates Toll-like receptor 4 (TLR4) in different immune cells, including macrophages [4]. LPS has been linked to several diseases including sepsis, acute lung injury, asthma, and atherosclerosis; thus, the signals it elicits in the host cell, although incompletely described, are of great biomedical significance.

The THP-1 monocytic human leukaemia cell line is a validated model to investigate monocyte and macrophage functions, mechanisms, and immune signalling pathways. In order to study the effects of LPS exposure, these cells can be used as monocytes or differentiated into THP-1 derived macrophages (TDM), by exposure to a pro-inflammatory stimulus prior to LPS stimulation [5]. Notably, the capability of LPS to induce gene expression in THP-1 derived macrophages was compared with the LPS-triggered response of human primary, peripheral blood mononuclear cell (PBMC) derived macrophages. The study concluded that although THP-1 cells are transformed and immortalised, their LPS-induced gene expression signature remains very similar to primary macrophages [6]. This model is reliable, simple and suitable for the investigation of inflammation-related macrophage responses [5] and thus it was selected for this study.

After the LPS challenge, the macrophage cell machinery is confronted with different activations that ultimately lead to a cellular phenotype switching. Specifically, TDM stimulation by LPS triggers different pro-inflammatory pathways within the cell through different effector proteins, namely MyD88 and TRIF [7], and also through a cytosolic protein complex known as NLRP3 inflammasome [8]. LPS also induces important remodelling of the cellular metabolism in macrophages, including glycogen metabolism [9] and a strong enhancement of glycolysis [10]. The increase in glycolysis products has the potential to burst the de novo biosynthesis of fatty acids, and to promote the expansion of the endoplasmic reticulum (ER) and Golgi to accommodate the increased demand for the synthesis, transport and secretion of inflammatory cytokines and chemokines. Thus, LPS triggers a complex response within the cell that requires a metabolic reprogramming at the expense of cellular energy provided by the increase in uptake of different molecules such as glucose, amino acids and fatty acids. It is known that lipids and their metabolism play an important role in ensuring macrophage plasticity throughout this process [11].

The aim of this work was to develop and validate a method with the capacity to provide at a glance a global picture depicting the biochemical changes occurring in an in vitro model of inflammation, in our case LPS-stimulated TDM. Specifically, methods able to detect in intact cells changes in protein, lipid and sugar/glycan composition in a non-time-consuming way could be useful to this scope.

In this perspective, Fourier transform infrared (FTIR) microspectroscopy has proven to be a powerful tool to monitor, in a non-destructive and label-free way, the global biochemical composition of whole cells, through the absorption of electromagnetic radiation in the mid infrared range. This vibrational tool probes a large number of molecules simultaneously, thus its sensitivity to structural and compositional changes makes it complementary to other biochemical methods [12,13]. For these reasons, FTIR spectroscopy has become an attractive tool in molecular and cellular biophysics with important applications also in biomedical research [13–19]. Given the complexity of cell spectra resulting from the overlapping absorptions of cell lipids, proteins, nucleic acids and carbohydrates, their interpretation requires a sophisticated multivariate analysis able to point out significant and non-redundant information [15,18,20].

Here, we describe the use of FTIR microspectroscopy coupled to Partial Least Squares-Discriminant Analysis (PLS-DA) to investigate in situ the biochemical modifications occurring in human TDM cells treated with LPS. The results of the multivariate analysis highlighted the most significant spectral components affected by the treatment, ascribable mainly to lipid and protein bands, thus stressing the fundamental role of these classes of molecules in inflammation and in immune response.

## 2. Results and Discussion

The biochemical modifications occurring in TDM cells exposed to LPS were investigated by FTIR microspectroscopy. In particular, we employed PLS-DA to compare FTIR data obtained from intact TDM treated with LPS at different time points over the course of 24 h, with data obtained from non-treated TDM. This multivariate analysis allowed not only the evaluation of the statistical significance of the observed spectral differences,

but also the identification of the spectral components responsible for the discrimination between treated and untreated cells, also taking into account the period of LPS exposure. The analysis has been performed on the second derivative spectra that have been calculated to better resolve the overlapped components in the absorption bands (Figure S1), necessary for the identification of peak positions and their assignment to the vibrational modes of the different molecules [13,18,20].

Figure 1 shows the Euclidean distance values of the PLS-DA projections of TDM cells treated with LPS and zero-time untreated cells (0 h), considering both the different spectral ranges and the period of incubation with LPS. The two-ways repeated-measurement ANOVA analysis indicates that the distances between treated and untreated TDM cells were significant for all the spectral regions and times considered (Figure 1).

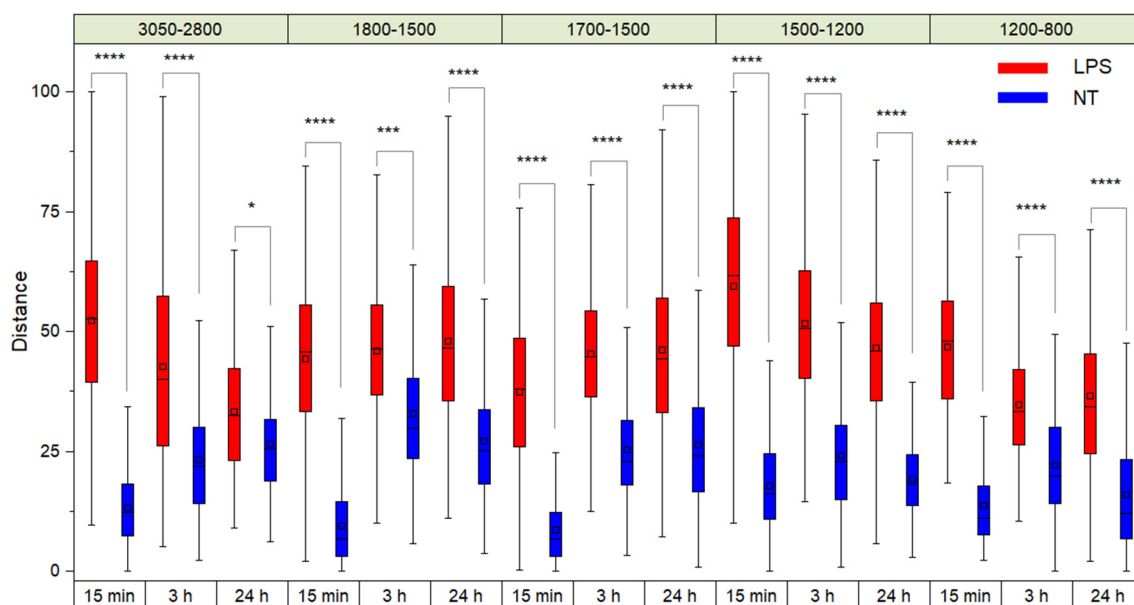


**Figure 1.** Euclidean distance values of the PLS-DA projections of TDM cells treated with LPS and non-treated cells (NT) for time zero analyses (0 h). The black horizontal line within the box is the median, the square within the box is the mean, the box ends show the first (Q1) and third (Q3) quartiles, the lower whisker is computed as the maximum value between the absolute minimum and  $Q1 - 1.5 \times IQR$ , and the upper whisker is the minimum between the absolute maximum and  $Q3 + 1.5 \times IQR$ . Here, IQR is the interquartile range computed as  $Q3 - Q1$ . Stars (\*, \*\*\*, \*\*\*\*) indicate the statistical significance evaluated by a two-ways repeated-measurement ANOVA analysis.

All the above considered, in the following figures, where the mean second derivative spectra are displayed, we will discuss mainly the spectral components responsible for the PLS-DA discrimination between LPS-treated and untreated TDM cells (only the components with overall weight factor  $\geq 75\%$  were considered). In the Supplementary Table S1 the assignment of the peaks identified in the analysed spectral ranges has been reported. To visualize the separation of the LPS treated (24 h) and untreated (0 h and 24 h) cells, the PLS-DA score plots have been reported in the Figure S2. The PLS-DA discrimination performance, evaluated using the classification accuracy, has been shown in the following figures as box-plots.

### 2.1. FTIR Analysis of Protein Secondary Structure Modifications in TDM Cells Exposed to LPS

Figure 2 reports the second derivative analysis of the Amide I band, in the  $1700\text{--}1600\text{ cm}^{-1}$  range, due to the C=O stretching vibration of the peptide bond, which provides information on the secondary structures of the whole cell proteins [21,22]. Untreated cells second derivative spectrum (0 h) was characterised by a component at  $\sim 1655\text{ cm}^{-1}$ , which arises from  $\alpha$ -helix and random coil structures and a component at  $\sim 1639\text{ cm}^{-1}$ ,

which can be assigned to  $\beta$ -sheets [21,22]. After 15 min of LPS treatment, a downshift of the  $\beta$ -sheet band (to  $\sim 1637\text{ cm}^{-1}$ ) was detected (see also loading plot of Figure 2), accompanied by the appearance of a shoulder at lower wavenumbers that can be assigned to intermolecular  $\beta$ -sheets, typical of protein aggregates and/or protein–protein interactions ([19,23,24] and references cited therein). Then, starting from 3 h of treatment with LPS, and up to the end of our observation (24 h), an increased intensity in the  $\alpha$ -helix/random coil band at  $\sim 1655\text{ cm}^{-1}$  was found, together with the disappearance of the shoulder at  $\sim 1628\text{ cm}^{-1}$  (see the loading plot of Figure 2). Moreover, in particular in the 24 h LPS-treated spectrum, a decreased intensity in the  $1638\text{ cm}^{-1}$  band was also detected (see the loading plot of Figure 2). Notably, 15 min after LPS administration, PLS-DA identified the spectral component at  $\sim 1628\text{ cm}^{-1}$ , typical of protein aggregates and/or protein–protein interactions, as the most relevant for the discrimination (overall weight 100%).

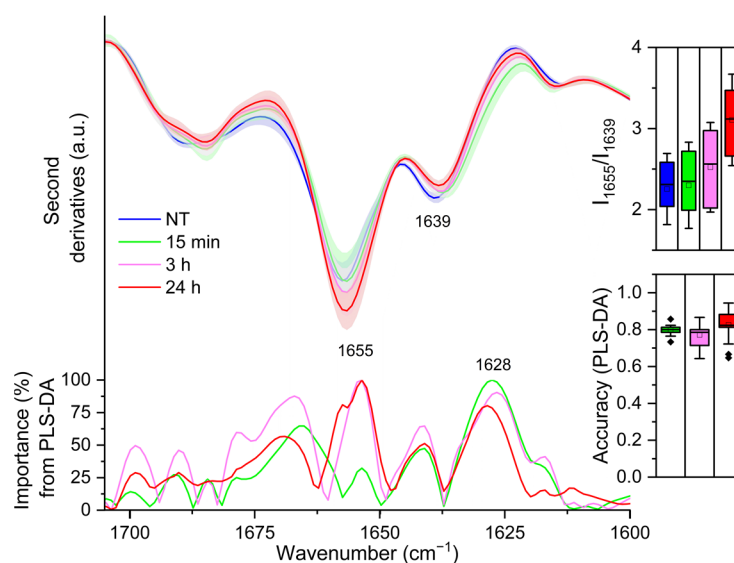


**Figure 2.** Mean second derivative spectra in the Amide I band of THP-1 cells before (0 h) and at different time points of LPS treatment. Standard deviation has also been displayed as a shadowed area. In the inset, the intensity ratio between the  $1655\text{ cm}^{-1}$  and the  $1639\text{ cm}^{-1}$  peaks, taken from the second derivatives, is illustrated. Below, the wavenumber importance for PLS-DA discrimination performed in the  $1700\text{--}1600\text{ cm}^{-1}$  spectral range is shown. The PLS-DA discrimination accuracy has been also reported. Box plots are given as in Figure 1.

The increase in the  $\alpha$ -helix band intensity (see also the inset of Figure 2) that we observed in the 3 h (overall weight 100%) and 24 h (overall weight 100%) spectra, accompanied by a further downshift of the  $\beta$ -sheet band, might be diagnostic of LPS-induced expression of proteins with both  $\alpha$ -helix and  $\beta$ -sheet structures.

Overall, our findings indicate that LPS stimulation induces significant global changes in the protein content, and likely also in the protein–protein interactions that in the IR spectra can be detected as changes in the whole cell protein secondary structures.

These results are in agreement with Meijer et al. [25] proteomic analysis that showed that LPS stimulation leads to significant up-regulation of a cluster of pro-inflammatory proteins, including the pro-inflammatory proteins macrophage migration inhibitory factor (MIF) and TNF- $\alpha$ , and various pro-inflammatory chemokines. The increased expression of several chemokines points to an important role of LPS-stimulated macrophages in recruiting other immune cells to sites of inflammation. Another upregulated functional cluster consists of proteins involved in actin cytoskeleton organisation, migration, chemotaxis and phagocytosis, as well as in transduction of LPS-induced TLR4 signalling and MHC-II mediated antigen presentation [25]. Proteoglycans (PGs)—glycosylated proteins, which have covalently attached glycosaminoglycans (GAGs)—are also known to be produced as extracellular and cell surface proteoglycans in response to LPS stimulation [26]. Moreover,

Dhungana et al. [27] reported a stimulus-induced statistically significant global increase in the number of distinct proteins in rafts in LPS-stimulated RAW macrophages. Authors described an LPS-induced dynamic exchange of proteasome subunits in macrophage triggered by LPS, which is thought to be “targeted” to lipid rafts in host cells in part through its interactions with raft-resident proteins (i.e., CD14). Specifically, they suggest that during LPS exposure a substantial number of new (i.e., basally raft-excluded) proteins are recruited to rafts in a time-dependent manner. Our observations about protein–protein interactions could pair with their data that collectively provide evidence for the localization of proteasome subunits to rafts, their reorganisation within rafts following LPS exposure, and an associated functional change in proteasomal activity specific to rafts that occurs during LPS signalling [27].

Interestingly, the appearance of the  $1628\text{ cm}^{-1}$  shoulder might be associated with the interaction of LPS with the TLR4/MD-2 complex situated on the plasma membrane to initiate the MyD88-dependent signalling. It has been reported that the activation of this pathway involves the formation of an intracellular oligomeric signalling complex called the myddosome, formed by MyD88 and members of the IRAK family [28]. Furthermore, another supramolecular organising centre (SMOC) can be attributed to LPS signalling through TLR4, which is the triffosome. LPS bound to TLR4/MD-2 and CD14 receptors undergoes internalisation in the endosome where it triggers the TRIF-dependent through the assembly of a complex of TRAM and TRIF [29].

## 2.2. FTIR Analysis of Lipid Modifications in TDM Cells upon Exposure to LPS: Insights from the $1500\text{--}1200\text{ cm}^{-1}$ and $3050\text{--}2800\text{ cm}^{-1}$ Spectral Ranges

The infrared absorption of TDM cells in the  $1500\text{--}1200\text{ cm}^{-1}$  spectral range is mainly due to the absorption of methyl and methylene groups from different biomolecules, including lipid hydrocarbon chains and head groups [22,30,31]. Moreover, the absorption of phosphate groups mainly from nucleic acids and lipids also occurs in this spectral range, as indicated by the broad band at  $\sim 1240\text{ cm}^{-1}$ , which is assigned to the antisymmetric phosphate (PO<sub>2</sub><sup>-</sup>) stretching mode [22,30–32]. Notably, comparing the NT (0 h) sample with LPS-treated cells spectra, PLS-DA identified as relevant—at each time point—only the component at  $\sim 1467\text{ cm}^{-1}$  (Figure 3a), mainly ascribable to the overlapping absorption of CH<sub>2</sub> and CH<sub>3</sub> groups from lipid hydrocarbon chains [22,30,31]. The intensity of this component, higher in the NT (0 h) cells, decreases rapidly at 15 min, and then increases again up to 24 h.

To investigate more in detail the effects of LPS on THP-1 derived macrophage lipids, FTIR analysis has been extended to the  $3050\text{--}2800\text{ cm}^{-1}$  spectral range, dominated by the absorption of lipid hydrocarbon chains. As shown in Figure 3b, the spectrum of untreated cells (0 h) was characterised by four main absorption bands:  $\sim 2921\text{ cm}^{-1}$  and  $2852\text{ cm}^{-1}$ , due to the antisymmetric and symmetric stretching of CH<sub>2</sub>; the  $\sim 2959\text{ cm}^{-1}$  and  $2872\text{ cm}^{-1}$ , due to the asymmetric and symmetric stretching of CH<sub>3</sub> [22,30,31].

The CH<sub>2</sub> bands decreased in intensity at 15 min of LPS treatment, and then increased again at 3 h, up to 24 h. In the inset of the Figure 3a, the ratio between the intensity of the CH<sub>2</sub> and CH<sub>3</sub> bands [33,34] is shown. The increase in this ratio, which is significant at 24 h post LPS treatment, is ascribable to the formation of longer hydrocarbon chains, in agreement with the spectral profile variation in the  $\sim 1467\text{ cm}^{-1}$  band discussed above (see Figure 3a). In addition, this result is also supported by the spectral changes displayed by the C=O band at  $\sim 1742\text{ cm}^{-1}$ , whose intensity, compared to that of untreated cells (0 h), decreased at 15 min and then increased again up to 24 h (see the insert of Figure S3). This absorption is mainly associated with the stretching vibrations of lipid ester groups [22,30,31].

As will be further discussed in the next section (see also Table S1), these results indicate that LPS stimulation induced a modification of the physicochemical properties of cell lipids. Interestingly, recent discoveries point to a complex metabolic network during macrophage activation, particularly regarding macrophage immunometabolism from the perspective

of the metabolism of lipids (reviewed by Batista-Gonzalez et al. [35]). In particular, it has been reported that the cell membrane lipid constituents, including glycerophospholipids and sphingolipids, are essential in modulating the pathogen recognition, and alterations in these molecules have been reported in LPS stimulated cells [11,36]. Among these, it has been speculated that some sphingolipids could have a crucial role in the regulation of the early pro-inflammatory or late pro-resolution phases of TLR4 activation [37]. Furthermore, phospholipids play a crucial role in cell-mediated inflammatory responses, including LPS-induced inflammation, since they are important signalling molecules involved in the regulation of cytokine production and because they provide precursors for the synthesis of potent lipid mediators [38]. Recent experimental evidence suggests that LPS-stimulated macrophages increase their fatty acid synthesis to store increased amounts of triacylglycerols and cholesterol esters in lipid droplets [39]. This synthesis appears to be required for T-cell priming [40], inflammasome activation [41] and pro-inflammatory cytokine production [39,40].

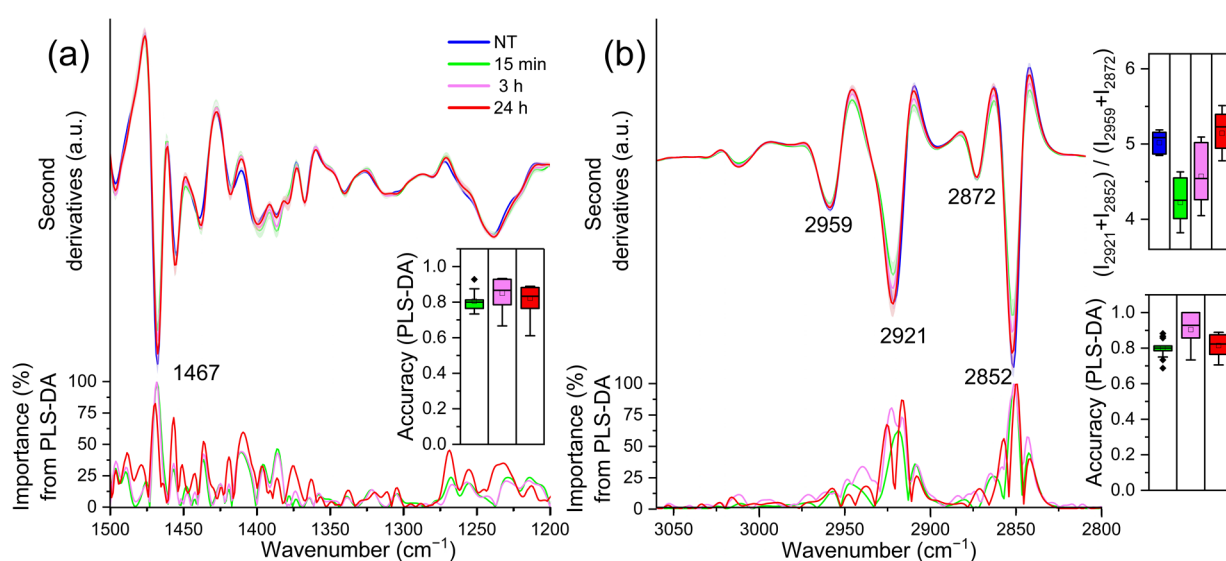


**Figure 3.** Mean second derivative spectra in the 1500–1200  $\text{cm}^{-1}$  (a) and 3050–2800  $\text{cm}^{-1}$  (b) ranges of TDM cells before (0 h) and at different time points of LPS treatment. Standard deviation has also been displayed as a shadowed area. Below, the wavenumber importance for PLS-DA discrimination performed in the selected spectral range is shown for each panel. In the insets, the PLS-DA discrimination accuracy (panels (a,b)) and the intensity ratio among the  $\text{CH}_2$  and the  $\text{CH}_3$  peaks (panel (b)) are reported. Box plots are given as in Figure 1.

### 2.3. FTIR Analysis of TDM Exposed to LPS: Analysis of the Fingerprint Region

The 1200–800  $\text{cm}^{-1}$  spectral range, the so-called fingerprint, is a very crowded and highly overlapped region of the spectrum, being dominated by the absorption of complex carbohydrate modes, isolated and/or associated or bound to other molecules, with important contributions also from lipids and nucleic acids. For this reason, the band assignment in this spectral range is not easy, and sometimes, not unequivocal. Overall, as we will describe below, the spectral components pulled out by PLS-DA are mostly ascribable to saccharides (including also GAGs) and lipids, in particular phospholipids and sphingomyelin (SM, Table S1).

Examining the loading plot relative to 15 min and 3 h of LPS treatment, PLS-DA brought out only one component carrying the higher spectral variance between treated and untreated cells: the  $\sim 1172 \text{ cm}^{-1}$  (overall weight  $\sim 100$ ) (see the loading plot of Figure 4), which decreased in intensity at 15 min upon LPS incubation, and then increased again up to 3 h (see Figure 4). As mentioned above, the assignment of this band is not immediate due to the overlapping contributions of different components. Considering its intensity

variation, which is synchronous with that of other bands assigned to lipid moieties, we tentatively assign it mainly to the CO-O-C stretching vibrations of phospholipids [22,30]. Moreover, it has been also associated with the C-OH and C-C stretching and C-O-H bending of carbohydrates [42,43] and with the SO<sub>4</sub> and C-O-S stretching of glycosaminoglycans (GAGs), such as heparin and heparan sulphate [44,45]. GAGs are highly heterogeneous linear macromolecules made up of a repeating disaccharide unit, with a variable number of sulphates. They are not only typical extracellular matrix components, but are also present in the cell membrane and as intracellular granules [46]. Considering that GAGs associated with proteoglycans (PGs) are known to play a crucial role in immune defence, being also involved in cytokine and chemokine regulation [47], we cannot exclude also a contribution of these complex molecules to the ~1172 cm<sup>-1</sup> absorption.

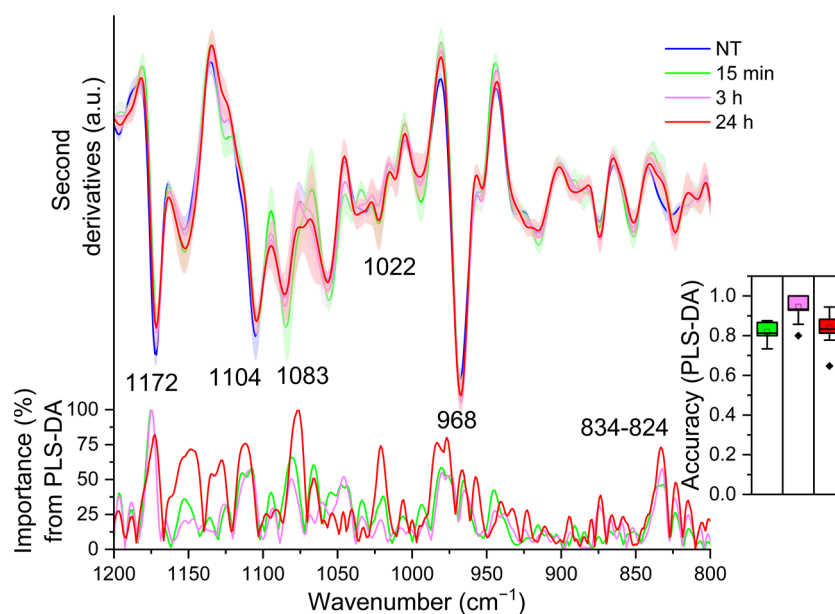


**Figure 4.** Mean second derivative spectra in the 1200–800 cm<sup>-1</sup> range of TDM cells before (0 h) and at different time points of LPS treatment. Standard deviation has also been displayed as a shadowed area. Below, the wavenumber importance for PLS-DA discrimination performed in the 1200–800 cm<sup>-1</sup> spectral range is shown. The PLS-DA discrimination accuracy has been also reported in the inset. Box plot is given as in Figure 1.

Noteworthy, PLS-DA relative to 24 h of treatment (see the loading plot of Figure 4) depicts a more complex scenario. The analysis, indeed, disclosed different components responsible for the classification: in addition to the ~1172 cm<sup>-1</sup> band (overall weight ~75%), displaying again a lower intensity compared to NT cells but similar to that of LPS-3 h, PLS-DA identified two more components that occurred at higher intensities in the 24 h treated cells compared to untreated cells (0 h): at ~1022 cm<sup>-1</sup> and ~968 cm<sup>-1</sup> (both with an overall weight ~75%). The first band is ascribable mainly to the ring vibrations and stretching vibrations of C-OH from side groups and C-O-C from glycosidic bonds of polysaccharides [42,43], being also typical of glycosylated proteins [48] and lipids [49]. The ~1022 cm<sup>-1</sup> band falls in a spectral range associated also with the vibrations of GAG pyranose ring structures [44]. Then, considering again the simultaneous variation in intensity of other absorption bands associated with lipids, we assign the component at ~968 cm<sup>-1</sup> mainly to the asymmetric stretching of the N(CH<sub>3</sub>)<sub>3</sub> group [30], which is characteristic not only of phosphatidylcholine (PC) but also of the sphingolipid sphingomyelin. In particular, sphingolipids do not just form the building blocks of eukaryotic cell membranes, but they also play a significant role in regulating cell functions. In this regard, Olona et al. reported that LPS induces the biosynthesis of sphingolipids that promote TLR4 signalling in macrophages [37]. We should add that we cannot exclude also a contribution of the C-C

stretching of the DNA backbone and/or of RNA ribose-phosphate main chain vibrations to the  $\sim 968\text{ cm}^{-1}$  absorption [32].

Furthermore, PLS-DA identified two other significant components that displayed a higher intensity in untreated cells (0 h) compared to 24 h: the component around  $1104\text{ cm}^{-1}$  (overall weight  $\sim 75\%$ ) and that at  $\sim 1083\text{--}1073\text{ cm}^{-1}$  (overall weight  $\sim 100\%$ ). The assignment of these bands is particularly difficult, because in this spectral window the absorption of phosphates, mainly from nucleic acids and lipids [30,32], is dominant as well as that of polysaccharides [50]. Indeed, these absorptions are also associated with different vibrational modes from polysaccharide rings, including the ones from GAGs, such as hyaluronic acid [44,51]. Notably, the  $\sim 1083\text{--}1073\text{ cm}^{-1}$  band is also assigned to the symmetric phosphate (PO<sub>2</sub><sup>-</sup>) stretching mode typical, for instance, of phospholipids and sphingomyelin [30].

Even if its overall weight is lower than 75% ( $\sim 73\%$ ), we should also mention the  $\sim 834\text{ cm}^{-1}$  component detected in untreated cells (0 h) and downshifted to  $\sim 824\text{ cm}^{-1}$  in 24 h treated cells, where it is also more resolved, which might reflect structural differences in the glycosidic linkages of polysaccharides by being assigned mainly to C1-H ring vibrations [43,52]. Moreover, this absorption has been also assigned to the C-O-S vibrations from GAGs [53,54].

Overall, the fingerprint analysis on one hand supports the importance of the physico-chemical variations in lipids triggered by LPS, as discussed above; on the other, it sheds light on a possible involvement of glycan modifications that could impact on the cell mechanical properties, which in turn may contribute to higher phagocytosis activity [55]. In addition, the observed changes, upon LPS stimulation, in sulfated sugars could be associated with the biosynthesis of sulfated glycosphingolipids or GAGs that are known to be endogenous ligands for the TLR4/MD-2 complex [56].

### 3. Materials and Methods

#### 3.1. Cell Maintenance

THP-1 X-Blue™ cells (InvivoGen, San Diego, CA, USA) were cultured in RPMI 1640, 2 mM L-glutamine, 10% heat-inactivated foetal bovine serum and 100 U/mL-100 µg/mL of Penicillin-Streptomycin and maintained at 37 °C, 5% CO<sub>2</sub>, 95% humidity. Cells were kept at a density of  $0.5 \times 10^6$  cells/mL by splitting them every three days. Media and supplements were purchased from Euroclone (Pero, Italy).

#### 3.2. Cell Differentiation

THP-1 X-Blue™ monocytes were seeded in 100 mm cell culture dishes (Corning, Corning, France),  $5 \times 10^6$  cells per dish in 10 mL of medium, and differentiated to TDM by exposure to 100 ng/mL of phorbol 12-myristate 13-acetate (PMA, InvivoGen, San Diego, CA, USA) for 3 days, as previously described [57,58]. Monocyte-to-macrophage differentiation was assessed by optical microscopy inspection. Macrophage-like cells adhered to the support and displayed a flattened and elongated morphology compared to floating round-shaped monocytes. Following differentiation, the PMA containing medium was removed and replaced by PMA-free fresh medium immediately prior to treatment.

#### 3.3. Cell Stimulation and Treatments

TDM were stimulated with 100 ng/mL of *Escherichia coli* 055:B5 LPS (Sigma-Aldrich, St Louis, USA) throughout different exposure periods, 15 min, 3 h and 24 h. After exposure to LPS, dishes were placed on ice and the medium removed. Cells were then washed with PBS (Euroclone), scraped using a cell scraper and collected into centrifuge tubes. After centrifugation at 4 °C for 10 min at approximately  $125 \times g$ , PBS was discarded and cell pellets were resuspended in physiological solution (NaCl 0.9%) for further centrifugation at 4 °C, 5 min at  $125 \times g$ . This washing step was repeated 3 times to ensure no medium contamination. Afterwards live cells were resuspended in 10 µL of physiological solution immediately prior to FTIR measurements.



### 3.4. FTIR Microspectroscopy Analysis of Intact THP-1 Derived Macrophage-Like Cells

About 3  $\mu\text{L}$  of cell suspension were deposited onto a  $\text{BaF}_2$  window, transparent to IR, and dried at room temperature for at least 30 min to eliminate the excess of water. FTIR absorption spectra were acquired in transmission mode, in the  $4000\text{--}700\text{ cm}^{-1}$  spectral range, by a Varian 610-IR infrared microscope coupled to the Varian 670-IR FTIR spectrometer (both from Varian Australia Pty Ltd., Mulgrave VIC, Australia), equipped with a mercury cadmium telluride nitrogen-cooled detector. The variable microscope aperture was adjusted to  $\sim 100\text{ }\mu\text{m} \times 100\text{ }\mu\text{m}$  (spatial resolution). Measurements were performed at  $2.0\text{ cm}^{-1}$  spectral resolution; 25 KHz scan speed, triangular apodization, and by the accumulation of 512 scan co-additions. Then, spectra were normalised at the Amide I band area for comparison (Figure S1) and the second derivative analysis was performed (after a 13-point smoothing of the measured spectra) by the Savitzky–Golay method (3rd polynomial, 9 smoothing points), using the GRAMS/32 software (Galactic Ind. Corp., Salem, NH, USA). Absolute peak intensities cannot be obtained from second derivative spectra, where peak height is proportional to the original height and inversely proportional to the square of the original half-width at half-height. However, under the condition that the original absorption spectra are of high quality, second derivatives can be used to monitor spectral changes if the very same analyses are performed on the original data [59,60].

For each sample, we collected several spectra by selecting different areas on the same sample through the variable diaphragm aperture of the infrared microscope. Furthermore, to evaluate the reproducibility of the results, we performed at least three independent experiments.

### 3.5. Multivariate Analysis

Multivariate analysis has been performed using R version 3.6.3. FTIR spectra have been split into five spectral regions and partial least square discriminant analysis (PLS-DA) has been applied on each region, as previously described [34].

PLS-DA is a widely used multidimensional linear regression method, which is a variant of the classical partial least square method when the dependent variable is categorical [61]. To assess the predictive discrimination and avoid over-fitting, for each method a 3-time repeated 5-fold cross-validation was applied; so, for each method, 15 models were trained. Since each sample has multiple spectra, folds have been created at the sample level, ensuring that all spectra for a given sample are either in the training or in the test set. More specifically, having  $N$  samples each with  $m_N$  spectra, on every round of cross-validation, the samples have been partitioned into 5 folds. Four folds (containing  $N*4/5$  samples) have been used to train the model, and the remaining fold (containing  $N*1/5$  samples) was used to test the model. Folds are complementary (i.e., no repeated samples in different folds) and the samples are randomly chosen. The training of the model is repeated 5 times, each time varying the test partition. The 5-fold cross-validation is then repeated 3-times to lower the risk of partition-dependent artefacts. The best model has been selected using the “one standard error rule”. In this case, the model with the best performance value is identified, and using resampling, we can estimate the standard error of performance. The final model used was the simplest model within one standard error of the (empirically) best model [62]. As a performance measure the root mean square error (RMSE) was used. For the PLS-DA method the variable importance measure here is based on weighted sums of the absolute regression coefficients [62]. Each PLS-DA model includes the following 3 classes: NT-T 0 h, NT-Tn, LPS-Tn. Different models have been created for each time: 15 min, 3 h, and 24 h. The discrimination accuracy among the classes was evaluated using the classification accuracy, e.g., the proportion of true results (true positive + true negative) over the total number of samples.

The distribution of distances between TDM cells treated with LPS and untreated has been obtained by computing the Euclidean distance between all pairs of spectra (in the low dimensional PLS score space), between group T 0 h and Tn for NT and for LPS, that is:

$$D(K)_{i,j} = \frac{1}{L} \sqrt{\sum_{c=1}^C (x_i^c - x_j^c)^2}$$

where  $i$  is the  $i$ -th spectra belonging to the initial time (T 0 h) group, while  $j$  is the  $j$ -th spectra belonging to the Tn (where  $n = 15 \text{ min}, 3 \text{ h}, 24 \text{ h}$ ) group.  $L$  is the number of PLS scores, and  $c$  is the  $C$ -th PLS component.  $K$  is either NT or LPS. In order to assess the statistical significance of the difference between the distances in NT and LPS and in the time factor, a two-ways repeated measurement ANOVA has been performed.

#### 4. Conclusions

The state-of-the-art understanding of LPS signalling is almost certainly incomplete and oversimplified due to the high complexity of the triggered events. The main aim of this work was to obtain a snapshot of the molecular events sparked by LPS stimulation in macrophage-like cells and dissect the molecular components specific of the inflammatory state and of the initiation of the innate immunity signalling in the cell through FTIR microspectroscopy supported by PLS-DA.

The FTIR analysis of intact macrophage cells, a non-destructive, non-time consuming and label-free method to measure the main molecular changes occurring in cells, proved to be the appropriate strategy to achieve our goal. Although FTIR analyses of other inflammation models have been published [63,64], this is, to the best of our knowledge, the first report in which FTIR is applied to study the complex molecular effects caused by LPS stimulation in human macrophages.

Within our global picture of inflammation in TDM, main findings are represented by the identification of different classes of molecules that stand out as the most affected by LPS stimulation. First, the changes in cell protein secondary structures, reflecting changes in protein content and interactions, as the time course evolves, might agree with cell phenomena related to pathway activation, cytokine production and also to proteasome targeted to lipid rafts on the host cell membrane, as described. Second, the significant intensity variation of a few bands ascribable to lipid moieties emphasises their role in the modulation of innate immune response and, therefore, the importance of some lipid molecules as markers of the inflammatory response [37,38]. Notably, the association of lipid metabolism and content inside the cell is a subject that has been far less described than inflammation-related proteins. Indeed, we observed significant differences in the lipid content during 24 h of LPS stimulation, which is congruent with recent research that correlates lipid metabolism and inflammation, showing that lipids can also be a reliable biomarker of inflammation.

Finally, the variations of the IR fingerprint spectral profile upon LPS stimulation also suggest a change in sulfated sugars that could be associated with the biosynthesis of sulfated glycosphingolipids and/or GAGs. In this regard, recent data show that glycosphingolipid sulphates are endogenous ligands for the TLR4/MD-2 complex [56]. Moreover, GAGs play a crucial role in the recruitment and control of a wide range of innate/cellular immune system regulatory proteins [47,65].

In conclusion, our study enabled the untargeted identification of IR spectroscopic markers outlining the cellular effects of LPS stimulation in human macrophages. The establishment of a combination of distinct features, in the form of specific marker bands that describe the initiation of the inflammatory response, has the potential to become a tool to assess, within a single analysis, those global biochemical changes related to an inflammatory stimulus, which can be another synthetic or natural pro-inflammatory TLR4 agonist, different than LPS. Moreover, with the same approach, it could also be possible to perform analyses to evaluate the anti-inflammatory potential of synthetic and natural

immunomodulators. Furthermore, our time course approach paired with the assignment of these spectroscopic markers to specific biomolecule classes allowed us to obtain information about the timing of the molecular events that occur after LPS administration. In addition, one of the advantages of our FTIR-based approach is the possibility to identify a priori specific classes of biomolecules associated with a biological event that could be the subject of further investigation, thus aiding basic research, decreasing time and resource consumption. Indeed, the strength of our approach is the possibility of obtaining an integrated view of functional changes using an untargeted analysis instead of focusing on a small set of markers or functions.

Although technological advances are needed to make the proposed FTIR method a large-scale screening tool, our study shows that FTIR microspectroscopy actually provides a broad view of the molecular events associated with LPS stimulation of macrophages and is able to detect those markers that are specific of the initiation of the cell-mediated immune response.

**Supplementary Materials:** The following supporting information can be downloaded at: <https://www.mdpi.com/article/10.3390/ijms232113447/s1>.

**Author Contributions:** Conceptualization, D.A., F.P. and A.N.; Methodology—cell manipulation protocol development, V.A.; Investigation—cell treatment, A.R.F.; Investigation—FTIR microspectroscopy, D.A.; Investigation—spectroscopic data analyses, D.A., P.M. and A.N.; Writing—original draft preparation, D.A., A.R.F., V.A., F.P. and A.N.; Writing—review and editing, all authors; Visualisation—graphical abstract, A.R.F. and V.A.; Supervision, F.P. and A.N.; Funding Acquisition, F.P. and A.N. All authors have read and agreed to the published version of the manuscript.

**Funding:** This research was funded by the European Union’s Horizon 2020 research and innovation programme under the Marie Skłodowska-Curie grant agreement No. 860325 (BactiVax), and by the University of Milano-Bicocca “Fondo di Ateneo per la Ricerca” (No. 2021-ATE-0438).

**Institutional Review Board Statement:** Not applicable.

**Informed Consent Statement:** Not applicable.

**Data Availability Statement:** The data that support the findings of this study are available from the corresponding author upon reasonable request.

**Acknowledgments:** D.A. acknowledges the support by a post doc research fellow (Assegno di Ricerca) of the University of Milano-Bicocca. F.P. acknowledges the CINMPIS consortium. Graphical Abstract created with BioRender.com.

**Conflicts of Interest:** The authors declare no conflict of interest. The funders had no role in the design of the study; in the collection, analyses, or interpretation of data; in the writing of the manuscript; or in the decision to publish the results.

## References

1. Takeuchi, O.; Akira, S. Pattern Recognition Receptors and Inflammation. *Cell* **2010**, *140*, 805–820. [[CrossRef](#)] [[PubMed](#)]
2. Viola, A.; Munari, F.; Sánchez-Rodríguez, R.; Scolaro, T.; Castegna, A. The Metabolic Signature of Macrophage Responses. *Front. Immunol.* **2019**, *10*, 1462. [[CrossRef](#)] [[PubMed](#)]
3. Rodríguez-Prados, J.-C.; Través, P.G.; Cuenca, J.; Rico, D.; Aragonés, J.; Martín-Sanz, P.; Cascante, M.; Boscá, L. Substrate Fate in Activated Macrophages: A Comparison between Innate, Classic, and Alternative Activation. *J. Immunol. Baltim. Md 1950* **2010**, *185*, 605–614. [[CrossRef](#)] [[PubMed](#)]
4. Fitzgerald, K.A.; Kagan, J.C. Toll-like Receptors and the Control of Immunity. *Cell* **2020**, *180*, 1044–1066. [[CrossRef](#)] [[PubMed](#)]
5. Chanput, W.; Mes, J.J.; Wichers, H.J. THP-1 Cell Line: An in Vitro Cell Model for Immune Modulation Approach. *Int. Immunopharmacol.* **2014**, *23*, 37–45. [[CrossRef](#)]
6. Sharif, O.; Bolshakov, V.N.; Raines, S.; Newham, P.; Perkins, N.D. Transcriptional Profiling of the LPS Induced NF-KB Response in Macrophages. *BMC Immunol.* **2007**, *8*, 1. [[CrossRef](#)]
7. Rossetti, C.; Peri, F. (Eds.) *The Role of Toll-like Receptor 4 in Infectious and Non Infectious Inflammation*; Progress in Inflammation Research; Springer International Publishing: Cham, Switzerland, 2021; Volume 87, ISBN 978-3-030-56318-9.
8. Swanson, K.V.; Deng, M.; Ting, J.P.-Y. The NLRP3 Inflammasome: Molecular Activation and Regulation to Therapeutics. *Nat. Rev. Immunol.* **2019**, *19*, 477–489. [[CrossRef](#)]

9. Ma, J.; Wei, K.; Liu, J.; Tang, K.; Zhang, H.; Zhu, L.; Chen, J.; Li, F.; Xu, P.; Chen, J.; et al. Glycogen Metabolism Regulates Macrophage-Mediated Acute Inflammatory Responses. *Nat. Commun.* **2020**, *11*, 1769. [[CrossRef](#)]
10. Regdon, Z.; Robaszekiewicz, A.; Kovács, K.; Rygielska, Ž.; Hegedűs, C.; Bodoor, K.; Szabó, É.; Virág, L. LPS Protects Macrophages from AIF-Independent Parthanatos by Downregulation of PARP1 Expression, Induction of SOD2 Expression, and a Metabolic Shift to Aerobic Glycolysis. *Free Radic. Biol. Med.* **2019**, *131*, 184–196. [[CrossRef](#)]
11. Zhang, C.; Wang, Y.; Wang, F.; Wang, Z.; Lu, Y.; Xu, Y.; Wang, K.; Shen, H.; Yang, P.; Li, S.; et al. Quantitative Profiling of Glycerophospholipids during Mouse and Human Macrophage Differentiation Using Targeted Mass Spectrometry. *Sci. Rep.* **2017**, *7*, 412. [[CrossRef](#)]
12. Ami, D.; Natalello, A.; Doglia, S.M. Fourier Transform Infrared Microspectroscopy of Complex Biological Systems: From Intact Cells to Whole Organisms. *Methods Mol. Biol.* **2012**, *895*, 85–100. [[CrossRef](#)] [[PubMed](#)]
13. Baker, M.J.; Trevisan, J.; Bassan, P.; Bhargava, R.; Butler, H.J.; Dorling, K.M.; Fielden, P.R.; Fogarty, S.W.; Fullwood, N.J.; Heys, K.A.; et al. Using Fourier Transform IR Spectroscopy to Analyze Biological Materials. *Nat. Protoc.* **2014**, *9*, 1771–1791. [[CrossRef](#)] [[PubMed](#)]
14. Mantsch, H.H. The Evolution of Biomedical Vibrational Spectroscopy: A Personal Perspective. *Biomed. Spectrosc. Imaging* **2015**, *4*, 315–329. [[CrossRef](#)]
15. Mantsch, H.H. Biomedical Vibrational Spectroscopy in the Era of Artificial Intelligence. *Molecules* **2021**, *26*, 1439. [[CrossRef](#)]
16. Miller, L.M.; Dumas, P. From Structure to Cellular Mechanism with Infrared Microspectroscopy. *Curr. Opin. Struct. Biol.* **2010**, *20*, 649–656. [[CrossRef](#)]
17. Finlayson, D.; Rinaldi, C.; Baker, M.J. Is Infrared Spectroscopy Ready for the Clinic? *Anal. Chem.* **2019**, *91*, 12117–12128. [[CrossRef](#)]
18. Morais, C.L.M.; Lima, K.M.G.; Singh, M.; Martin, F.L. Tutorial: Multivariate Classification for Vibrational Spectroscopy in Biological Samples. *Nat. Protoc.* **2020**, *15*, 2143–2162. [[CrossRef](#)]
19. Ami, D.; Mereghetti, P.; Natalello, A. Contribution of Infrared Spectroscopy to the Understanding of Amyloid Protein Aggregation in Complex Systems. *Front. Mol. Biosci.* **2022**, *9*, 822852. [[CrossRef](#)]
20. Ami, D.; Doglia, S.M.; Mereghetti, P. *Multivariate Analysis for Fourier Transform Infrared Spectra of Complex Biological Systems and Processes*; IntechOpen: London, UK, 2013.
21. Barth, A. Infrared Spectroscopy of Proteins. *Biochim. Biophys. Acta-Bioenerg.* **2007**, *1767*, 1073–1101. [[CrossRef](#)]
22. Tamm, L.K.; Tatulian, S.A. Infrared Spectroscopy of Proteins and Peptides in Lipid Bilayers. *Q. Rev. Biophys.* **1997**, *30*, 365–429. [[CrossRef](#)]
23. Seshadri, S.; Khurana, R.; Fink, A.L. Fourier Transform Infrared Spectroscopy in Analysis of Protein Deposits. *Methods Enzymol.* **1999**, *309*, 559–576. [[CrossRef](#)] [[PubMed](#)]
24. Natalello, A.; Doglia, S.M.; Carey, J.; Grandori, R. Role of Flavin Mononucleotide in the Thermostability and Oligomerization of Escherichia Coli Stress-Defense Protein WrbA. *Biochemistry* **2007**, *46*, 543–553. [[CrossRef](#)] [[PubMed](#)]
25. Meijer, K.; Weening, D.; de Vries, M.P.; Priebe, M.G.; Vonk, R.J.; Roelofsen, H. Quantitative Proteomics Analyses of Activation States of Human THP-1 Macrophages. *J. Proteom.* **2015**, *128*, 164–172. [[CrossRef](#)] [[PubMed](#)]
26. Kolseth, I.B.M.; Reine, T.M.; Vuong, T.T.; Meen, A.J.; Fan, Q.; Jenssen, T.G.; Grønning-Wang, L.M.; Kolset, S.O. Serglycin Is Part of the Secretory Repertoire of LPS-Activated Monocytes. *Immun. Inflamm. Dis.* **2015**, *3*, 23–31. [[CrossRef](#)] [[PubMed](#)]
27. Dhungana, S.; Merrick, B.A.; Tomer, K.B.; Fessler, M.B. Quantitative Proteomics Analysis of Macrophage Rafts Reveals Compartmentalized Activation of the Proteasome and of Proteasome-Mediated ERK Activation in Response to Lipopolysaccharide. *Mol. Cell. Proteom.* **2009**, *8*, 201–213. [[CrossRef](#)] [[PubMed](#)]
28. Balka, K.R.; De Nardo, D. Understanding Early TLR Signaling through the Myddosome. *J. Leukoc. Biol.* **2019**, *105*, 339–351. [[CrossRef](#)]
29. Kieser, K.J.; Kagan, J.C. Multi-Receptor Detection of Individual Bacterial Products by the Innate Immune System. *Nat. Rev. Immunol.* **2017**, *17*, 376–390. [[CrossRef](#)]
30. Casal, H.L.; Mantsch, H.H. Polymorphic Phase Behaviour of Phospholipid Membranes Studied by Infrared Spectroscopy. *BBA-Rev. Biomembr.* **1984**, *779*, 381–401. [[CrossRef](#)]
31. Lewis, R.N.A.H.; McElhaney, R.N. Fourier Transform Infrared Spectroscopy in the Study of Lipid Phase Transitions in Model and Biological Membranes. Practical Considerations. In *Methods in Molecular Biology*; Dopico, A.M., Ed.; Humana Press: Totowa, NJ, USA, 2007; pp. 207–226. ISBN 978-1-59745-519-0.
32. Banyay, M.; Sarkar, M.; Gräslund, A. A Library of IR Bands of Nucleic Acids in Solution. *Biophys. Chem.* **2003**, *104*, 477–488. [[CrossRef](#)]
33. Dučić, T.; Stamenković, S.; Lai, B.; Andjus, P.; Lučić, V. Multimodal Synchrotron Radiation Microscopy of Intact Astrocytes from the HSOD1 G93A Rat Model of Amyotrophic Lateral Sclerosis. *Anal. Chem.* **2019**, *91*, 1460–1471. [[CrossRef](#)]
34. Ami, D.; Duse, A.; Mereghetti, P.; Cozza, F.; Ambrosio, F.; Ponzini, E.; Grandori, R.; Lunetta, C.; Tavazzi, S.; Pezzoli, F.; et al. Tear-Based Vibrational Spectroscopy Applied to Amyotrophic Lateral Sclerosis. *Anal. Chem.* **2021**, *93*, 16995–17002. [[CrossRef](#)] [[PubMed](#)]
35. Batista-Gonzalez, A.; Vidal, R.; Criollo, A.; Carreño, L.J. New Insights on the Role of Lipid Metabolism in the Metabolic Reprogramming of Macrophages. *Front. Immunol.* **2020**, *10*, 2993. [[CrossRef](#)] [[PubMed](#)]

36. Lee, J.W.; Mok, H.J.; Lee, D.Y.; Park, S.C.; Kim, G.-S.; Lee, S.-E.; Lee, Y.-S.; Kim, K.P.; Kim, H.D. UPLC-QqQ/MS-Based Lipidomics Approach To Characterize Lipid Alterations in Inflammatory Macrophages. *J. Proteome Res.* **2017**, *16*, 1460–1469. [[CrossRef](#)] [[PubMed](#)]
37. Olona, A.; Hateley, C.; Muralidharan, S.; Wenk, M.R.; Torta, F.; Behmoaras, J. Sphingolipid Metabolism during Toll-like Receptor 4 (TLR4)-mediated Macrophage Activation. *Br. J. Pharmacol.* **2021**, *178*, 4575–4587. [[CrossRef](#)] [[PubMed](#)]
38. Conde, T.A.; Mendes, L.; Gaspar, V.M.; Mano, J.F.; Melo, T.; Domingues, M.R.; Duarte, I.F. Differential Modulation of the Phospholipidome of Proinflammatory Human Macrophages by the Flavonoids Quercetin, Naringin and Naringenin. *Molecules* **2020**, *25*, 3460. [[CrossRef](#)]
39. Castoldi, A.; Monteiro, L.B.; van Teijlingen Bakker, N.; Sanin, D.E.; Rana, N.; Corrado, M.; Cameron, A.M.; Hässler, F.; Matsushita, M.; Caputa, G.; et al. Triacylglycerol Synthesis Enhances Macrophage Inflammatory Function. *Nat. Commun.* **2020**, *11*, 4107. [[CrossRef](#)]
40. Everts, B.; Amiel, E.; Huang, S.C.-C.; Smith, A.M.; Chang, C.-H.; Lam, W.Y.; Redmann, V.; Freitas, T.C.; Blagih, J.; van der Windt, G.J.W.; et al. TLR-Driven Early Glycolytic Reprogramming via the Kinases TBK1- $IKK\epsilon$  Supports the Anabolic Demands of Dendritic Cell Activation. *Nat. Immunol.* **2014**, *15*, 323–332. [[CrossRef](#)]
41. Moon, J.-S.; Lee, S.; Park, M.-A.; Siempos, I.I.; Haslip, M.; Lee, P.J.; Yun, M.; Kim, C.K.; Howrylak, J.; Ryter, S.W.; et al. UCP2-Induced Fatty Acid Synthase Promotes NLRP3 Inflammasome Activation during Sepsis. *J. Clin. Investig.* **2015**, *125*, 665–680. [[CrossRef](#)]
42. Gazi, E.; Dwyer, J.; Lockyer, N.P.; Gardner, P.; Shanks, J.H.; Roulson, J.; Hart, C.A.; Clarke, N.W.; Brown, M.D. Biomolecular Profiling of Metastatic Prostate Cancer Cells in Bone Marrow Tissue Using FTIR Microspectroscopy: A Pilot Study. *Anal. Bioanal. Chem.* **2007**, *387*, 1621–1631. [[CrossRef](#)]
43. Kacuráková, M. FT-IR Study of Plant Cell Wall Model Compounds: Pectic Polysaccharides and Hemicelluloses. *Carbohydr. Polym.* **2000**, *43*, 195–203. [[CrossRef](#)]
44. Brézillon, S.; Untereiner, V.; Lovergne, L.; Tadeo, I.; Noguera, R.; Maquart, F.X.; Wegrowski, Y.; Sockalingum, G.D. Glycosaminoglycan Profiling in Different Cell Types Using Infrared Spectroscopy and Imaging. *Anal. Bioanal. Chem.* **2014**, *406*, 5795–5803. [[CrossRef](#)] [[PubMed](#)]
45. Mohamed, H.T.; Untereiner, V.; Cinque, G.; Ibrahim, S.A.; Götte, M.; Nguyen, N.Q.; Rivet, R.; Sockalingum, G.D.; Brézillon, S. Infrared Microspectroscopy and Imaging Analysis of Inflammatory and Non-Inflammatory Breast Cancer Cells and Their GAG Secretome. *Molecules* **2020**, *25*, 4300. [[CrossRef](#)] [[PubMed](#)]
46. Makatsori, E.; Karamanos, N.K.; Papadogiannakis, N.; Hjerpe, A.; Anastassiou, E.D.; Tseggenidis, T. Synthesis and Distribution of Glycosaminoglycans in Human Leukemic B- and T-Cells and Monocytes Studied Using Specific Enzymic Treatments and High-Performance Liquid Chromatography. *Biomed. Chromatogr.* **2001**, *15*, 413–417. [[CrossRef](#)] [[PubMed](#)]
47. Taylor, K.R.; Gallo, R.L. Glycosaminoglycans and Their Proteoglycans: Host-associated Molecular Patterns for Initiation and Modulation of Inflammation. *FASEB J.* **2006**, *20*, 9–22. [[CrossRef](#)] [[PubMed](#)]
48. Derenne, A.; Derfoufi, K.-M.; Cowper, B.; Delporte, C.; Goormaghtigh, E. FTIR Spectroscopy as an Analytical Tool to Compare Glycosylation in Therapeutic Monoclonal Antibodies. *Anal. Chim. Acta* **2020**, *1112*, 62–71. [[CrossRef](#)]
49. Kirschbaum, C.; Greis, K.; Mucha, E.; Kain, L.; Deng, S.; Zappe, A.; Gewinner, S.; Schöllkopf, W.; von Helden, G.; Meijer, G.; et al. Unravelling the Structural Complexity of Glycolipids with Cryogenic Infrared Spectroscopy. *Nat. Commun.* **2021**, *12*, 1201. [[CrossRef](#)]
50. Kačuráková, M.; Mathlouthi, M. FTIR and Laser-Raman Spectra of Oligosaccharides in Water: Characterization of the Glycosidic Bond. *Carbohydr. Res.* **1996**, *284*, 145–157. [[CrossRef](#)]
51. Pan, N.C.; Pereira, H.C.B.; da Silva, M.d.L.C.; Vasconcelos, A.F.D.; Celligoi, M.A.P.C. Improvement Production of Hyaluronic Acid by *Streptococcus Zoepidemicus* in Sugarcane Molasses. *Appl. Biochem. Biotechnol.* **2017**, *182*, 276–293. [[CrossRef](#)]
52. Synytsya, A. Fourier Transform Raman and Infrared Spectroscopy of Pectins. *Carbohydr. Polym.* **2003**, *54*, 97–106. [[CrossRef](#)]
53. Foster, A.B.; Martlew, E.F.; Stacey, M.; Taylor, P.J.M.; Webber, J.M. 236. Amino-Sugars and Related Compounds. Part VIII. Some Properties of 2-Deoxy-2-Sulphoamino-D-Glucose, Heparin, and Related Substances. *J. Chem. Soc. Resumed* **1961**, 1204–1208. [[CrossRef](#)]
54. Parker, F.S. *Applications of Infrared Spectroscopy in Biochemistry, Biology, and Medicine*; Springer US: Boston, MA, USA, 1971; ISBN 978-1-4684-1874-3.
55. Zhao, Y.; Mahajan, G.; Kothapalli, C.R.; Sun, X.-L. Sialylation Status and Mechanical Properties of THP-1 Macrophages upon LPS Stimulation. *Biochem. Biophys. Res. Commun.* **2019**, *518*, 573–578. [[CrossRef](#)] [[PubMed](#)]
56. Su, L.; Athamna, M.; Wang, Y.; Wang, J.; Freudenberg, M.; Yue, T.; Wang, J.; Moresco, E.M.Y.; He, H.; Zor, T.; et al. Sulfatides Are Endogenous Ligands for the TLR4-MD-2 Complex. *Proc. Natl. Acad. Sci. USA* **2021**, *118*, e2105316118. [[CrossRef](#)] [[PubMed](#)]
57. Artusa, V.; Ciaramelli, C.; D’Aloia, A.; Facchini, F.A.; Gotri, N.; Bruno, A.; Costa, B.; Palmioli, A.; Airoidi, C.; Peri, F. Green and Roasted Coffee Extracts Inhibit Interferon- $\beta$  Release in LPS-Stimulated Human Macrophages. *Front. Pharmacol.* **2022**, *13*, 806010. [[CrossRef](#)] [[PubMed](#)]
58. Facchini, F.A.; Minotti, A.; Luraghi, A.; Romerio, A.; Gotri, N.; Matamoros-Recio, A.; Iannucci, A.; Palmer, C.; Wang, G.; Ingram, R.; et al. Synthetic Glycolipids as Molecular Vaccine Adjuvants: Mechanism of Action in Human Cells and In Vivo Activity. *J. Med. Chem.* **2021**, *64*, 12261–12272. [[CrossRef](#)] [[PubMed](#)]

59. Zhang, J.; Yan, Y.-B. Probing Conformational Changes of Proteins by Quantitative Second-Derivative Infrared Spectroscopy. *Anal. Biochem.* **2005**, *340*, 89–98. [[CrossRef](#)]
60. Song, C.L.; Kazarian, S.G. Effect of Controlled Humidity and Tissue Hydration on Colon Cancer Diagnostic via FTIR Spectroscopic Imaging. *Anal. Chem.* **2020**, *92*, 9691–9698. [[CrossRef](#)]
61. Pérez-Enciso, M.; Tenenhaus, M. Prediction of Clinical Outcome with Microarray Data: A Partial Least Squares Discriminant Analysis (PLS-DA) Approach. *Hum. Genet.* **2003**, *112*, 581–592. [[CrossRef](#)]
62. Breiman, L.; Friedman, J.; Stone, C.J.; Olshen, R.A. *Classification and Regression Trees*; The Wadsworth and Brooks-Cole Statistics-Probability Series; Taylor & Francis: Abingdon-on-Thames, UK, 1984; ISBN 978-0-412-04841-8.
63. Dunkhunthod, B.; Talabnin, C.; Murphy, M.; Thumanu, K.; Sittisart, P.; Eumkeb, G. *Gymnema inodorum* (Lour.) Decne. Extract Alleviates Oxidative Stress and Inflammatory Mediators Produced by RAW264.7 Macrophages. *Oxidative Med. Cell. Longev.* **2021**, *2021*, 8658314. [[CrossRef](#)]
64. Paemane, A.; Rattanabunyong, S.; Ketngamkum, Y.; Siriwaseree, J.; Pongpamorn, P.; Romyanon, K.; Tangphatsornruang, S.; Kuaprasert, B.; Choowongkamon, K. Mass Spectrometry and Synchrotron-FTIR Microspectroscopy Reveal the Anti-inflammatory Activity of Bua Bok Extracts. *Phytochem. Anal.* **2022**, *33*, 1086–1098. [[CrossRef](#)]
65. Hatano, S.; Watanabe, H. Regulation of Macrophage and Dendritic Cell Function by Chondroitin Sulfate in Innate to Antigen-Specific Adaptive Immunity. *Front. Immunol.* **2020**, *11*, 232. [[CrossRef](#)]